IET Optoelectronics

ORIGINAL RESEARCH PAPER

IET | The Institution of Engineering and Technology | WILEY

All-optical control of spatial beam intensity in multimode fibres by polarisation modulation

Omar F. Anjum (ORCID) | **Massimiliano Guasoni** | **Periklis Petropoulos**

Optoelectronics Research Centre, University of Southampton, Southampton, UK

Correspondence

Omar F. Anjum, Optoelectronics Research Centre, University of Southampton, Southampton, UK.
Email: o.f.anjum@soton.ac.uk

Abstract

The authors demonstrate that by injecting a combination of LP_{11} modes in a few-mode high-birefringence fibres that all-optical control of the spatial beam intensity at the fibre output is achieved by varying the polarisation at the fibre input. These results may be generalised to the cases where different and several higher order modes are employed.

1 | INTRODUCTION

Multimode fibres (MMFs) are used in a wide range of application areas encompassing telecommunications, medicine and astronomy [1–3]. As a result, efficient methods for the characterisation of the modal properties of MMFs have been proposed and demonstrated [4–6]. In the last decade, researchers have demonstrated the ability to achieve deterministic control over the output state (polarisation plus spatial) of light by computing the transfer matrix of a MMF. This powerful approach can be used even when the fibre is subject to random mode coupling, which is the case for typical weak-birefringent fibres longer than a few meters. This method relies on experimental data gathered by carrying out multiple-input multiple-output measurements so as to identify the input launching conditions that provide a specific modal distribution and state-of-polarisation (SOP) at the fibre output [7–10].

Techniques that achieve robust manipulation of the spatial modes coupled into a few-mode fibre offer new opportunities for all-optical, ultrafast modulation of higher order-modes in space-division-multiplexing, where each mode-frequency pair may be associated with an independent information channel (see, for example [11–14]). Such systems could also be used in time/frequency division multiplexing to modulate (receive) in time or frequency at different higher order modes at the transmitter (receiver) side [15]. Moreover, by launching any number of higher order modes in addition to the LP_{11} group,

one may obtain a variety of complex spatial intensity patterns controlled through the input polarisation, which may be used in a number of applications beyond communications. For example, the ability to create deterministic spatial shapes may be advantageous in microscopy, in which the region of interest can be isolated from its surrounding by shaping an incident beam [16, 17]. Furthermore, the ability to predictably map input-output relations through fibres is of importance in areas such as endoscopic imaging and spectroscopy [18, 19].

The authors build on the general framework of existing methods, but offer a new perspective which relies on the use of a highly birefringent fibre to achieve a simpler and more predictable way of manipulating the spatial intensity distribution at the fibre output. Differently from previous works based on isotropic or random (weakly) birefringent fibres, here the high birefringence fully decouples the orthogonal linear polarisations. This brings about two main outcomes. Firstly, a fully analytical formula linking the input SOP and the output spatial intensity distribution is found. Secondly, by simply switching the input polarisation from being linearly polarised along one fibre axis to the other, we are able to switch in time the spatial field intensity at the fibre output from being a pure LP_{11a} mode to a LP_{11b} mode. At the same time, a further configuration can be implemented which is fully insensitive to input SOP variations. These results could be generalised to higher order modes as well. In other words, we provide a simple and controllable technique for all-optical spatial intensity

modulation, which is based on linear polarisation switching and does not require any measurement of the fibre transfer matrix. The modulation is potentially ultrafast as it may be driven by a fast polarisation controller (PC) at the fibre input.

2 | THEORY

For simplicity, here we focus our attention on the propagation of LP_{11a} and LP_{11b} modes in a polarisation maintaining fibre, but the main outcomes could be generalised to the case where one or more higher order modes are employed. Note that due to the large fibre birefringence, LP_{11a} and LP_{11b} modes are non-degenerate, which strongly suppresses the random coupling. Excitation of these modes is possible by means of a holographic PP [20], which shapes an input beam into a two-lobed pattern which is then focused to the input facet of the fibre, as shown conceptually in the left/upper portion of Figure 1. Here, α denotes the angle between the reference frame $x'y'$ aligned with the (fixed) fibre birefringence axes and the (variable) PP axes xy. Hence, α determines the orientation of the PP. When $\alpha = 0$, modes LP_{11a} and LP_{11b} are identical in both frames. In contrast, Figure 2 illustrates the spatial modes in each frame when $\alpha \neq 0$.

In the $x'y'$ frame, the general expression for the input electric field $\mathbf{E}_{IN}$ can be written as a combination of linearly polarised LP_{11a} and LP_{11b} spatial modes aligned along the x' and the y' directions: $\mathbf{E}_{IN} = m'_a(i'_{ax} \cdot \mathbf{x}' + i'_{ay} \cdot \mathbf{y}') + m'_b(i'_{bx} \cdot \mathbf{x}' + i'_{by} \cdot \mathbf{y}')$. Here $m'_a(x, y)$ $(m'_b(x, y))$ represents the normalised transverse profile of the LP_{11a} (LP_{11b}) mode and the coefficients $\{i'_{ax}, i'_{ay}\}$ ($\{i'_{bx}, i'_{by}\}$) denote the input amplitudes
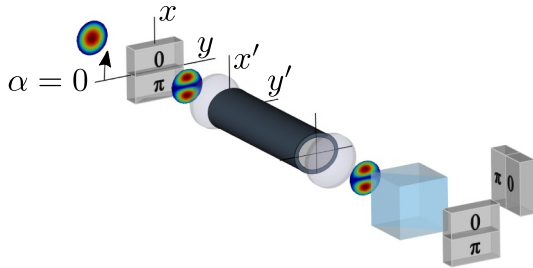
FIGURE 1 Conceptual illustration (also see text) showing a holographic phase plate (PP) being used to launch a combination of LP_{11a} and LP_{11b} modes into a birefringent fibre. Frame xy depends on PP angle α. The birefringence-axes frame $(x'y')$ is the laboratory frame
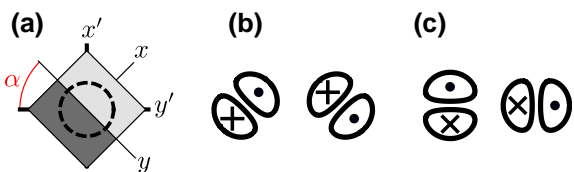
FIGURE 2 (a) Representation of the reference systems xy and $x'y'$, (b) LP_{11a} (left) and LP_{11b} (right) mode profiles in the xy reference system (dotted lobe is in anti-phase with crossed lobe) and (c) LP_{11a} (left) and LP_{11b} (right) mode profiles in the $x'y'$ reference system

of its x'- and y'-polarised components, respectively, whereas $\mathbf{x}'$ ($\mathbf{y}'$) is a unit vector along the x' (y') direction. Additionally, we indicate with $\mathbf{A}'_{IN} = [i'_{ax}\ i'_{ay}\ i'_{bx}\ i'_{by}]$ the vector of input amplitudes.

The same notation above applies for the frame xy with the substitutions $x' \to x, y' \to y, i' \to i, m' \to m$. In this frame, the field representation at the fibre input is particularly simple. Because the PP axis is the $\mathbf{y}$-axis, the field can be written as a combination of LP_{11a}-like modes only. Therefore $\mathbf{A}_{IN} = [i_{ax}\ i_{ay}\ 0\ 0]$, regardless of the value of α.

The relation between the vectors $\mathbf{A}_{IN}$ and $\mathbf{A}'_{IN}$ is defined by the matrix–vector product $\mathbf{A}'_{IN} = \mathbf{M}\mathbf{A}_{IN}$, such that $\mathbf{M}$ is the projection matrix defined as [21]:

$$\mathbf{M} = \begin{pmatrix} c^2 & -sc & -sc & s^2 \\ sc & c^2 & -s^2 & -sc \\ sc & -s^2 & c^2 & -sc \\ s^2 & sc & sc & c^2 \end{pmatrix} \begin{matrix} 11_{ay} \\ 11_{ax} \\ 11_{by} \\ 11_{bx} \end{matrix}$$

with $c = \cos(\alpha)$ and $s = \sin(\alpha)$.

During the propagation in the fibre, the amplitude of each mode accumulates a phase-shift that is defined by the product between its propagation constant and the fibre length L (any losses are assumed negligible). The output amplitude o'_{mn} reads therefore $o'_{mn} = \exp(jk_{mn}L) \cdot i'_{mn}$, where k_{mn} is its corresponding propagation constant. If we call $\mathbf{A}'_{OUT} = [o'_{ax}\ o'_{ay}\ o'_{bx}\ o'_{by}]$ the vector of the output modal amplitudes, we can then write $\mathbf{A}'_{OUT} = \mathbf{D}\mathbf{A}'_{IN}$, where $\mathbf{D}$ is the diagonal matrix diag($\exp(jk_{ax}L)$, $\exp(jk_{ay}L)$, $\exp(jk_{bx}L)$, $\exp(jk_{by}L)$) of the phase-shift terms.

The output modal amplitudes $\mathbf{A}_{OUT}$ in the original reference frame xy are finally computed as $\mathbf{A}_{OUT} = \mathbf{M}^{-1}\mathbf{A}'_{OUT} = \mathbf{M}^{-1}\mathbf{D}\mathbf{M}\mathbf{A}_{IN}$. This allows comparing the input and output amplitudes in the same reference frame xy. We denote the total output power coupled to the LP_{11m} mode (m $\in \{a, b\}$) as $P_m = |o_{mx}|^2 + |o_{my}|^2$. After some algebraic calculations, one can derive the useful relation

$$\begin{aligned} P_a = \ & S_0/4(2 + 2\cos^2 p + \sin^2 p \cos \Delta d_x + \sin^2 p \cos \Delta d_y) \\ & + S_1/4(\cos \Delta d_x - \cos \Delta d_y)\sin^3 p \\ & - S_3/4(\cos \Delta d_x - \cos \Delta d_y)\sin^2 p \cos p, \end{aligned} \tag{1}$$

where S_0, S_1 and S_3 are stokes parameters that define the input polarisation ($S_0 = |i_{ax}|^2 + |i_{ay}|^2$, $S_1 = i_{ax}i^*_{ay} + i_{ay}i^*_{ax}$ and $S_3 = |i_{ax}|^2 - |i_{ay}|^2$); $p = 2\alpha$; $\Delta d_x = (k_{ax} - k_{bx})L$; $\Delta d_y = (k_{ay} - k_{by})L$. A similar equation can be derived for P_b. Note that energy conservation holds true, that is to say, $S_0 = |i_{ax}|^2 + |i_{ay}|^2 \equiv P_a + P_b$.

The central result highlighted by Equation (1) is that the total output power coupled over the LP_{11a} and LP_{11b} modes depends on the input polarisation, the relative angle α among the PP and the fibre axes, as well as the fibre length L. Consequently, for a fixed and appropriate angle and length, we

can control these powers in time through the input polarisation, at a speed that is essentially determined by the PC.

Although Equation (1) provides a full characterisation of the output powers P_a and P_b as a function of the system parameters, it is interesting to illustrate in detail the instances $\alpha = 0$, $\alpha = \pi/2$ and $\alpha = \pi/4$, since they provide an intuitive picture of the role of the input polarisation in the control of P_a and P_b.

From Equation (1), we see that whenever the PP is aligned with one of the fibre axes ($\alpha = 0$ or $\alpha = \pi/2$), the output power $P_a = S_0$ is constant and independent of the input polarisation. Also, as shown in Figure 3, under this condition, the beam at the fibre input is fully aligned with the fibre axes. The high birefringence prevents any energy exchange among the components relating to the two axes, so that the output power remains fully coupled to the LP_{11a} mode.

On the contrary, when $\alpha = \pi/4$ (see Figure 4) the input power is equally split among the fibre axes, so that both the LP_{11a} and LP_{11b} modes of the fibre are excited. First consider the instance in which the input polarisation is parallel to the x'-axis of the fibre. In this case, the input field can be decomposed into t sum of two x'-polarised modes: $\mathbf{E}_{IN} = \mathbf{x}' \cdot (i'_{ax}m'_a + i'_{bx}m'_b)$. These two fibre modes have equal amplitudes and are in phase at the fibre input (Figure 4(a)), namely, $i'_{ax} = i'_{bx}$. Nevertheless, each of them accumulates a different phase delay in propagation. If the phase mismatch $\Delta d_x = (k_{ax} - k_{bx})L$ is an even multiple of π, then the modes add in phase at the fibre output, so no difference is observed with respect to the input field (Figure 4(b)), that is to say, $o'_{ax} = o'_{bx}$.

Now consider the case in which the input polarisation is parallel to the y'-axis so that $\mathbf{E}_{IN} = \mathbf{y}' \cdot (i'_{ay}m'_a + i'_{by}m'_b)$ (Figure 4(c)). Then, if the accumulated phase mismatch $\Delta d_y = (k_{ay} - k_{by})L$ is an odd multiple of π, the output modal amplitudes are now in anti-phase ($o'_{ax} = -o'_{bx}$) so that a $\pi/2$ rotation is observed with respect to the input field (see Figure 4(d)).

In summary, the example in Figure 4 points out the strong polarisation diversity of the system under analysis, which is in contrast to the case in Figure 3. With $\alpha = \pi/4$, when the input polarisation goes from linearly polarised along one fibre axis to the other (from x' to y' or vice versa), the output field undergoes a $\pi/2$ spatial rotation. More specifically, we switch from an output LP_{11a} mode aligned with the x-axis of the PP ($P_a = S_0$ and $P_b = 0$, Figure 4(b)), to an output LP_{11b} mode aligned with the y-axis of the PP ($P_a = 0$ and $P_b = S_0$, Figure 4 (d)). On the contrary, when $\alpha = 0$ or $\pi/2$, the output intensity distribution is polarisation insensitive and is unchanged from its input configuration (Figure 3).

These outcomes are consistent with Equation (1): under the conditions $\alpha = \pi/4$, $\Delta d_x = 2N\pi$ and $\Delta d_y = (2M + 1)\pi$, with N and M integers, and we find that $P_a = S_0/2 + S_1/2$ and $P_b = S_0/2 - S_1/2$. If the input polarisation is now aligned with the fibre axis x' (y'), then $S_1 = S_0$ ($S_1 = -S_0$), so finally $P_a = S_0$ and $P_b = 0$ ($P_a = 0$ and $P_b = S_0$). Note that a similar result is found when $\Delta d_x = (2M + 1)\pi$ and $\Delta d_y = 2N\pi$. Interestingly enough, the conditions set out above are necessary to observe a $\pi/2$ rotation of the output field. If any one of these
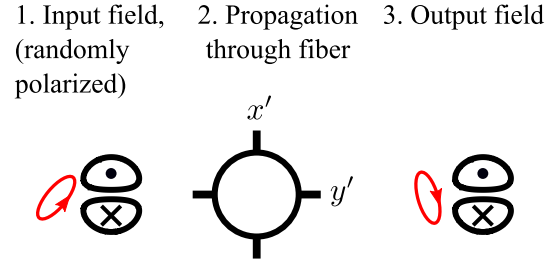
conditions is not met, then the $\pi/2$ rotation is not possible, whatever may be the input polarisation. Rather, in this case the typical output field is an out-of-phase combination of LP_{11a} and LP_{11b} modes, which gives rise to shapes that are intermediate between the pure LP_{11a} and LP_{11b} states, and the same can be observed later in experimental results.

The bandwidth of operation can also be estimated by taking into account the conditions discussed in our preceding analysis. In short, the bandwidth corresponds to the portion of spectrum where the phase-mismatch term Δd_x (and similarly, Δd_y) is nearly constant, that is, it is (nearly) independent of the frequency f. Note that $\Delta d_x(f) = \Delta n \cdot 2\pi f L/c$, where Δn is the fibre birefringence indicating the effective index difference between the x and y polarisations. The index contrast Δn depends on the frequency, however, it is typically preserved over a relatively large bandwidth (e.g. finite element simulations of

FIGURE 3 If $\alpha = 0$, spatial output is insensitive to input polarisation (likewise for $\alpha = \pi/2$)
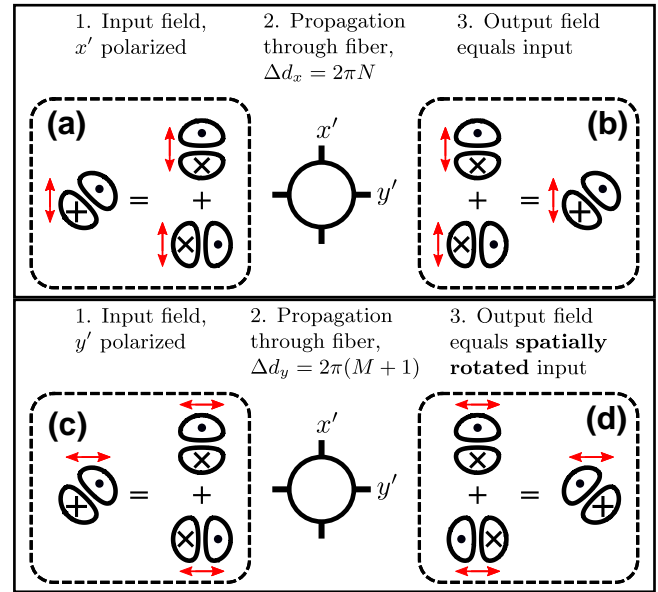

FIGURE 4 Polarisation-sensitive setup ($\alpha = \pi/4$). The fibre is such that $\Delta d_x = 2\pi N$, whereas $\Delta d_y = 2\pi(M + 1)$. (a) decomposition of the x'-polarised input field as the sum of m'_{ax} and m'_{bx}; (b) under the condition $\Delta d_x = 2\pi N$ the output fields m'_{ax} and m'_{bx} add in phase. The resulting output LP_{11} mode profile has the same spatial orientation as the input; (c) decomposition of the y'-polarised input field as the sum of m'_{ay} and m'_{by} and (d) under the condition $\Delta d_y = 2\pi(M + 1)$, the output fields m'_{ay} and m'_{by} add in anti-phase. The resulting output LP_{11} mode profile undergoes a $\pi/2$ rotation with respect to the input field

elliptical fibres suggest Δn is almost constant across the C-band). Therefore, the difference $d = \Delta d_x(f_1) - \Delta d_x(f_2)$ at two frequencies f_1 and f_2 reads $d = \Delta n \cdot 2\pi \cdot \Delta f \cdot L/c$, where $\Delta f = f_1 - f_2$. Also, whenever $d \ll 1$, the desired linear combination of output modes remains the same for all the frequencies that range from f_1 to f_2. More precisely, our numerical model (see Equation 1) suggests that under the condition $d < 0.2$ the output beam shape is well preserved. This condition finally reads as $\Delta f < 0.2c/(\Delta n \cdot 2\pi L)$, which sets the operation bandwidth $B = 0.2c/(\Delta n \cdot 2\pi L)$. In the case of the fibre under analysis, the beat-length at 1950 nm indicates that $\Delta n = 3.75 \times 10^{-4}$. Assuming the same value at 1530 nm and considering the fibre length is 3 m, we find a bandwidth as narrow as 8.5 GHz. One may, however, reduce the fibre length to the cm scale and/or employ fibres with a reduced birefringence so as to increase the bandwidth up to several THz (tens of nanometres in the C-band). While broadband operation is certainly desirable for telecom applications (e.g. space-division-multiplexing), some other applications may benefit from a narrow bandwidth (e.g. in sensing or spectroscopy to resolve specific, narrow spectral regions).

3 | EXPERIMENTAL SETUP

The setup shown in Figure 5 was used to experimentally test the ideas discussed above. A 1530-nm continuous wave diode laser was the light source and an (electronically) programmable, liquid crystal-based PC was used to control the polarisation of light into the fibre.

The fibre used for this experiment was a commercially available panda style PM fibre (Thorlabs Part Number PM2000). Having a core radius of 7 μm and a beat length of 5.2 mm at 1950 nm, it was specified for polarisation-maintained single-mode operation at wavelengths greater than 1850 nm. However, in the lower to mid C-band, it became possible to reliably guide the higher order spatial modes LP_{11a} and LP_{11b} with negligible loss over short lengths. The length of the fibre was 3 m. Rotators were used to align the principal polarisation axes of the fibre such that one of them was parallel to the plane of the optical bench and the other was perpendicular to it. This was done by means of a polarimetric technique [22] using broadband amplified spontaneous emission (ASE) from a C-band erbium doped fibre amplifier (EDFA). To excite the LP_{11} mode in the fibre, we used a holographic free-space phase-plate to shape the input beam into the
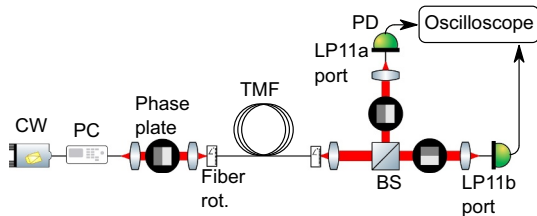
requisite phase profile [20]. The intensity profile of the collimated output beam was imaged on an infrared camera when required.

We used a beam-splitter (BS) cube to divide the output to two paths with perpendicularly oriented PPs (see Figures 1 and 5), with light from each focused into a single-mode fibre. The output PPs were rotated by the same angle α as the input PP. This allowed analysing the powers P_a and P_b coupled respectively to the LP_{11a} and LP_{11b} modes in the same xy reference system as the input PP.

The powers were monitored by means of a photo-detector (PD) and oscilloscope. Maximum (minimum) power was directed to an output port when the beam at the fibber output was composed of one of the LP_{11} spatial modes oriented along (perpendicular to) its PP axis. For example, the emerging output beam shown in Figure 1 will couple very strongly into the port that lies in its straight path.

4 | EXPERIMENTAL RESULTS

Both the polarisation insensitive and sensitive configurations illustrated in Figures 3 and 4 were tested experimentally. First, the input PP was aligned along either fibre axis ($\alpha = 0$ or $\pi/2$), thereby launching exclusively LP_{11a} or LP_{11b} into the fibre. Figure 6 shows the measured power at each LP_{11} port versus time when $\alpha = 0$ and the input polarisation was scrambled randomly using the PC. While the graph shows limited fluctuation in LP_{11a} power which can be ascribed to polarisation-dependent loss and imperfect alignment in the optical system, the difference in power between LP_{11a} and LP_{11b} exceeded 18 dB at all times. This agrees with our previous remark that if $\alpha = 0$ (or $\pi/2$), the system is polarisation insensitive. Consequently, the output spatial profile observed using an infrared camera and as shown in Figure 6, is fixed in time and aligned with one of the fibre axes.

Next, the PPs were aligned diagonally to the fibre axes, that is, $\alpha = \pm\pi/4$. This configuration proved to be polarisation sensitive. Figure 7 shows the variation of power at each port versus time, as the PC changes the input polarisation from being linearly polarised along one fibre axis (time t_1) to the other (time t_3) and then back. Also shown are
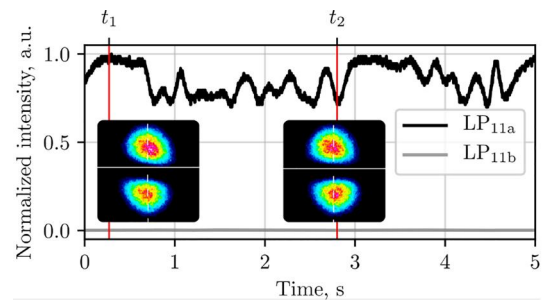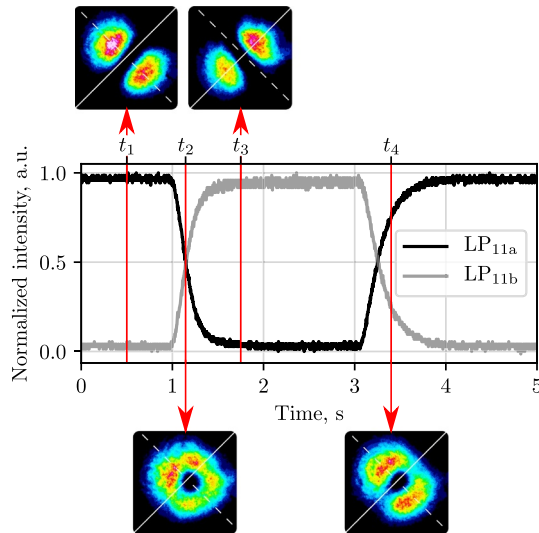

FIGURE 5 Experimental setup

FIGURE 6 Polarisation insensitive setup: the beam profiles of either of the spatial modes in the LP_{11} group are unchanged when input polarisation is varied

FIGURE 7 Polarisation sensitive setup: transfer in power between ports LP$_{11a}$ and LP$_{11b}$ due to change in polarisation

images of the output beam shape at various stages of the power transition. The fact that both the exchange of power between the two ports and the $\pi/2$ spatial rotation of the output beam were achieved by switching between the aforementioned states of polarisation is in agreement with our theoretical model. This polarisation sensitive configuration therefore allows implementing an all-optical spatial intensity modulation at the fibre output, which does not require any a-priori measurement of the fibre transfer matrix. The speed of the modulation is dictated by the input PC. Also note that, as discussed in the theoretical section, Δd_x (Δd_y) is nearly an even (odd) multiple of π. It should be noted that, for an ideal (straight) fibre, the phase mismatch terms Δd_x and Δd_y are fixed. However, by spooling the fibre with different radii of curvature, we can perturb the phase accumulated during propagation by each mode and therefore Δd_x and Δd_y can be changed. An optimum position which maximised the polarisation sensitivity of the system could be found easily, and enabled reaching a maximum power extinction ratio of 13 dB between the ports. As anticipated in the theory section, in the intermediate cases represented at times t_2 and t_4 in Figure 7, the beam resembled superpositions of out-of-phase LP$_{11a}$ and LP$_{11b}$ modes.

5 | CONCLUSIONS AND PERSPECTIVES

By using a highly birefringent fibre guiding the LP$_{11}$ group, we have demonstrated all-optical control of the output spatial intensity, which allows us to provide evidence of spatial intensity modulation in time. Differently from transfer-matrix approaches in weakly random birefringent fibres, here we derive a fully analytical formula that links the input SOP to the spatial intensity distribution at the fibre output. We identify two distinct configurations: the first is polarisation insensitive with

the PP oriented at 0 or $\pi/2$ and the second is polarisation sensitive with the PP oriented at $\pi/4$. In this last configuration, when the input light is switched from being linearly polarised along one fibre axis to the other, a $\pi/2$ rotation of the spatial field intensity is realised, and the output switches from a (pure) LP$_{11a}$ profile to LP$_{11b}$. The speed of this transition is determined by the speed of the PC, and could therefore be in the order of picoseconds. Importantly, this scheme can also be applied to other higher order modes, for example, to switch from LP$_{12a}$ to LP$_{12b}$, using the appropriate phase mask.

CONFLICT OF INTEREST

The authors declare no conflict of interest.

ORCID

Omar F. Anjum https://orcid.org/0000-0001-6229-4305

REFERENCES

1. Kahn, J.M., Miller, D.A.: Communications expands its space. Nat. Photon. 11(1), 5–8 (2017)
2. Ozbay, B.N., et al.: Three dimensional two-photon brain imaging in freely moving mice using a miniature fiber coupled microscope with active axial-scanning. Sci. Report. 8(1), 1–14 (2018)
3. Wright, L.G., et al.: Spatiotemporal dynamics of multimode optical solitons. Opt. Exp. 23(3), 3492–3506 (2015)
4. Fontaine, N.K., et al.: Laguerre-Gaussian mode sorter. Nat. Commun. 10(1), 1–7 (2019)
5. Carpenter, J., Eggleton, B.J., Schröder, J.: Comparison of principal modes and spatial eigenmodes in multimode optical fibre. Laser Photon. Rev. 11(1), 1600259 (2017)
6. Schulze, C., et al.: Mode coupling in few-mode fibers induced by mechanical stress. J. Lightw. Technol. 33(21), 4488–4496 (2015)
7. Carpenter, J., Eggleton, B.J., Schröder, J.: 110x110 optical mode transfer matrix inversion. Opt. Exp. 22(1), 96–101 (2014).
8. Xiong, W., et al.: Complete polarization control in multimode fibers with polarization and mode coupling. Light Sci. Appl. 7(1), 54 (2018)
9. Niederriter, R.D., Siemens, M.E., Gopinath, J.T.: Continuously tunable orbital angular momentum generation using a polarization-maintaining fiber. Opt. Lett. 41(14), 3213–3216 (2016)
10. Khan, S.N., Chatterjee, S.K., Chaudhuri, P.R.: Polarization and propagation characteristics of switchable first-order azimuthally asymmetric beam generated in dual-mode fiber. Appl. Opt. 54(6), 1528–1542 (2015)
11. Richardson, D.J., Fini, J.M., Nelson, L.E.: Space-division multiplexing in optical fibres. Nat. Photon. 7(5), 354–362 (2013)
12. Parmigiani, F., et al.: Elliptical core few mode fibers for multiple-input multiple output-free space division multiplexing transmission. IEEE Photon. Technol. Lett. 29(21), 1764–1767 (2017)
13. Rademacher, G., et al.: Long-haul transmission over few-mode fibers with space-division multiplexing. J. Lightw. Technol. 36(6), 1382–1388 (2018)
14. Randel, S., et al.: 6×56-gb/s mode-division multiplexed transmission over 33-km few-mode fiber enabled by 6×6 MIMO equalization. Opt. Exp. 19(17), 16697–16707 (2011)

15. Yan, S., et al.: Archon: a function programmable optical interconnect architecture for transparent intra and inter data center sdm/tdm/wdm networking. J. Lightw. Technol. 33(8), 1586–1595 (2015)

16. Heffernan, B.M., et al.: A fiber-coupled stimulated emission depletion microscope for bend-insensitive through-fiber imaging. Sci. Report. 9(1), 1–8 (2019)

17. Palomba, S., Novotny, L.: Near-field imaging with a localized nonlinear light source. Nano Lett. 9(11), 3801–3804 (2009)

18. Ploschner, M., Tyc, T., Cizmar, T.: Seeing through chaos in multimode fibres. Nat. Photon. 9(8), 529–535 (2015)

19. Redding, B., Cao, H.: Using a multimode fiber as a high-resolution, low-loss spectrometer. Opt. Lett. 37(16), 3384–3386 (2012)

20. Ryf, R., Bolle, C., von Hoyningen Huene, J.: Optical coupling components for spatial multiplexing in multi-mode fibers. In: European conference and exposition on optical communications. Optical Society of America, Geneva, Switzerland (2011). Th–12

21. Guasoni, M., Parmigiani, F., Horak, P., Fatome, J., Richardson, D.J.: Intermodal four-wave-mixing and parametric amplification in km-long multi-mode fibers. J. Lightw. Technol. 35(24), 5296–5305 (2017)

22. Poole, C.D., Favin, D.L.: Polarization-mode dispersion measurements based on transmission spectra through a polarizer. J. Lightw. Technol. 12(6), 917–929 (1994)